



3D Simulation of Basin-Edge Effects on the Ground Motion Characteristics

J. P. NARAYAN¹

SUMMARY

This paper presents 3D simulation of effects of basin-edge geometry on the characteristics of generated surface waves. The program used in simulations is based on parsimonious staggered grid finite difference approximation of 3D elastodynamic wave equations, with variable grid size. The double-couple point shear dislocation source, based on moment tensor formulation, was implemented into the numerical grid, instead of simple plane waves, so that effects of complex interactions of diffracted waves, mode converted waves and the transmitted body waves in the basin on the surface wave characteristics could be studied. The basin-edge models with different edge geometry and angle of incidence were simulated. The obtained results revealed surface wave generation near the basin-edge and their propagation normal to the edge, towards the basin.

Simulations with different edge-slopes along with spectral analysis revealed decrease of surface wave amplitude with slope. Generation of higher modes of surface waves was obtained in the of thicker soil layer. Large ground displacement near the basin-edge in some of the cases may be due to the interference of surface/diffracted waves with the direct waves and their multiples. Further, it was inferred that characteristics of surface wave very much dependent on radiation pattern on the basis of response of different angle of incidence. The simulated results along with observed intense concentration of damage parallel to the edge during past earthquakes revealed that basin-edge effects deserve a particular attention for earthquake resistant design and seismic microzonation.

INTRODUCTION

Surface waves, generally caused by lateral variation of material properties [elastic parameters and density], play an important role in damage during earthquakes in the sedimentary basins. Bard and his co-workers carried out a lot of numerical experiments to study the effects of basin-edge on surface wave generation and their characteristics using Aki-Larner method [Bard [1, 2, 3 & 4]] and finite difference method [Moczo [5]]. Further, a common conclusion has been drawn that later arrivals are primarily composed of surface waves generated at the basin-edge by examining the phase and group velocities, polarity and arrival azimuth [Horike [6]; Kinoshita [7]; Hatayama [8]; Kawase [9] and Pitarka [10]]. Narayan [11] reported that high frequency surface wave generation near the basin edge, when frequency

¹Assistant Professor, Department of Earthquake Engineering, Indian Institute of Technology Roorkee, Roorkee-247 667, INDIA, jaypnfeq@iitr.ernet.in

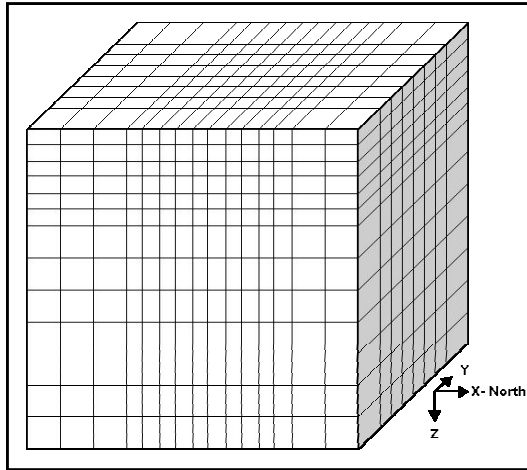


Fig. 1 Grid layout with variable grid spacing.

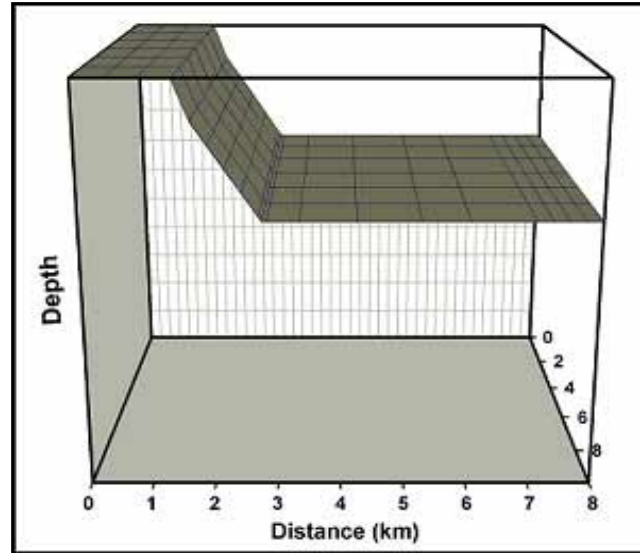


Fig. 2 Vertically exaggerated 3D basin-edge model

content in the body waves exceed the fundamental frequency of soil deposit. The high frequency surface waves generated at the basin-edge are of great interest in the field of engineering seismology. The Northridge earthquake [1994] and Kobe earthquake [1995] are the recent reminders that soft sediments and basin-edge have significant effects on surface wave generation and ground motion amplification.

Very fine grid finite difference mesh is essential, if one is interested to incorporate the effects of local geology in simulations, particularly geometrical lateral variations in material property, topography or very low velocity soil layer. Further, grid size is determined on the basis of the shortest wavelength of interest. So, in order to fulfill the challenging job of high frequency ground motion simulation a variable grid finite difference [FD] scheme as proposed by Miyatake [12] and recently used by Pitarka [13] is used in the computations [Fig. 1]. In the present study, algorithm developed by Narayan [14] with variable grid size was used for 3D simulation of basin-edge effects on surface wave generation. Double couple point shear dislocation source based on moment tensor source formulation was implemented into the numerical grid [Pitarka [13]; Narayan [14, 15]]. The seismic responses of the basin-edge models for different edge geometries and source locations were computed. Vacuum formulation at the free surface and sponge boundary condition on the model edges were implemented to avoid instability and edge reflections, respectively [Graves [16]; Israeli and Orszag [17]].

NUMERICAL SIMULATIONS

Seismic response of different basin-edge models were computed using an algorithm based on second order parsimonious staggered grid finite difference approximation of 3-D elastodynamic wave equation [Luo [18]; Ohminato [19]]. Double couple point shear dislocation source was implemented into the computational grid based on moment tensor source formulation [Pitarka [13] and Narayan [14, 15]].

Table 1. Different location of the double couple source (dip=90°, rake=15° and strike=30°).

Source site	Epicentral distance wrt the center of basin-edge	Focal depth (km)	Angle of incident
SL1	0.776 km, South	6.448	---
SL2	0.000 km	6.448	00.0 ⁰
SL3	3.224 km, North	5.584	30.0 ⁰
SL4	4.559 km, North	4.559	45.0 ⁰
SL5	5.584 km, North	3.224	60.0 ⁰

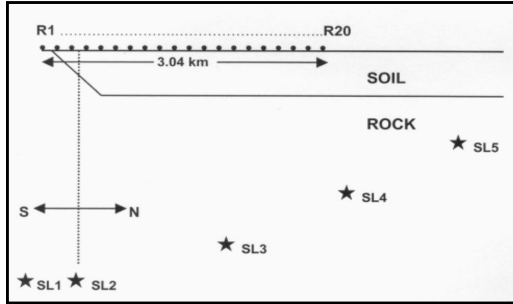


Fig. 3 Source-receiver configuration wrt source and basin-edge.

In most of the simulations, twenty-equidistant [160 m] receivers were used for recordings and their location with respect to the basin-edge is shown in figure 3. A double-couple source with focal mechanism dip= 90° , rake= 15° and strike= 30° was used in simulation.

The P- and S-waves velocities and densities were taken as 1800.0 m/s, 500.0 m/s and 2.0 g/cm^3 for soil and 3464.1 m/s, 2000.0 m/s and 2.5 g/cm^3 for half space [hard rock]. Variable grid size was used in the discretization of the basin-edge model [6.25 km X 5.25 km X 7.5 km]. The horizontal dimension of the grids in north-south direction from left edge of the model up to 2.0 km was 40 m, 16 m in between 2.0 km to 4.8 km and 40 m thereafter. Similarly, in the east-west direction, it was 40 m up to 1.0 km, 16 m between 1.0 km to 4.0 km and 40 m thereafter. In the vertical direction grid size was 16 m up to depth of 0.464 km and 40 m thereafter [Fig. 1].

The time step and

In the present study, vacuum formulation is adopted [α , β and $\rho \rightarrow 0$] in the region above the free surface since it requires careful consideration in numerical schemes for stability and accuracy. Sponge boundary condition was implemented on the model edges to avoid the edge reflections.

Two layered 3D basin-edge models with different soil thickness and edge-slopes were simulated [Fig. 2]. In all the cases, the surface position of basin-edge was fixed. In the simulation, positive x-coordinate was pointing in north direction and positive z-coordinate was pointing vertically downward. The southern basin-edge is elongated in the east-

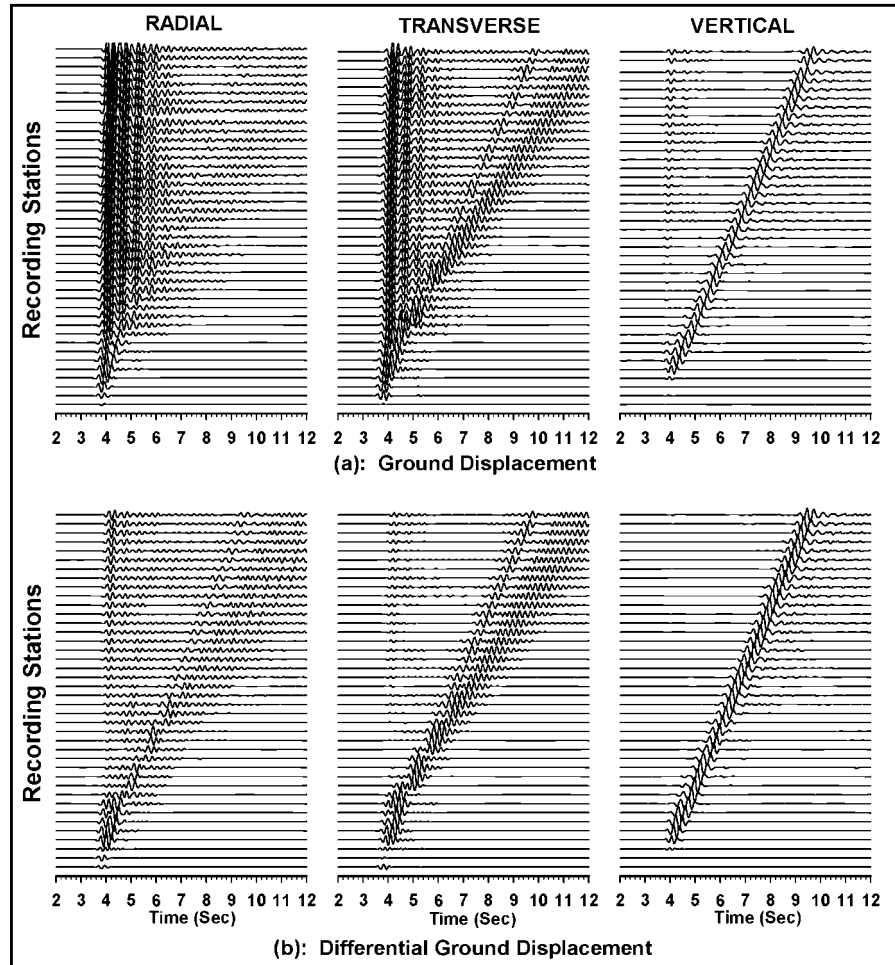


Fig. 4 Radial, transverse and vertical components of (a) ground displacement and (b) differential ground displacement at different receiver points corresponding to simulation of basin-edge model (soil thickness 128 m, slope 15°) using source SL2.

dominant frequency were taken as 0.002 s and 2.5 Hz respectively. The Ricker wavelet was used as an excitation function.

The basin-edge model with edge slope as 15° and soil thickness as 128 m was simulated using source location at SL2 [Table 1]. Radial, transverse and vertical components of ground displacement were computed at 41 equidistant [64m apart] receiver points, extending from basin-edge to 2.56 km north of edge. The different components of ground displacement and the differential ground displacement are shown in figures 4a and 4b, respectively [Note: Normalization factor for vertical components is five times larger than the normalization factor for radial and transverse components in all the other figures also]. Figure 4a shows body wave and their multiples with large apparent velocity along with seismic phases with much lesser apparent velocity. But, phases with lesser apparent velocity are not prominently identifiable in the radial component due to relatively small amplitudes and presence of longer chain of body wave multiples.

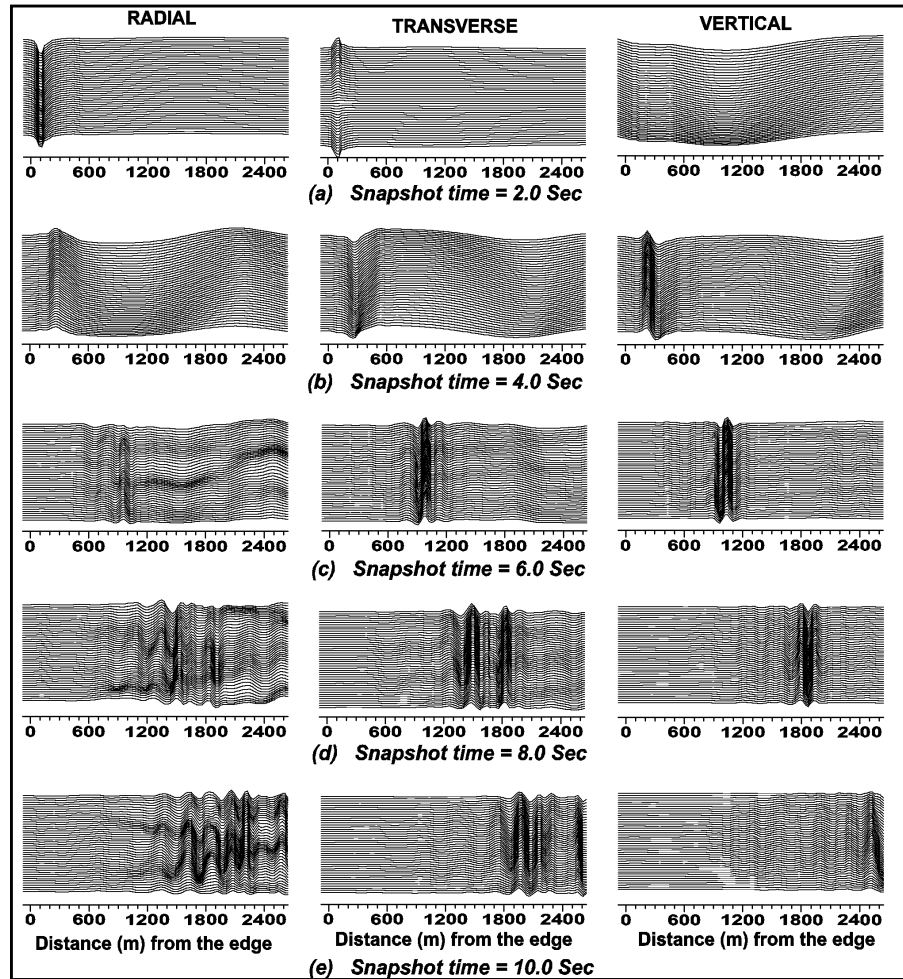


Fig. 5 snapshots at different times on the ground surface corresponding to the model and source position used in computation of response shown in figure 4. [Note: vertical scale is different for different snapshots]

To identify these seismic phases with lesser apparent velocity, differential ground motions were computed along the north-south direction. The differential ground displacements $\left(\frac{\partial u}{\partial x}, \frac{\partial v}{\partial x} \text{ and } \frac{\partial w}{\partial x}\right)$ were computed by

simply dividing the difference of ground displacements at two adjacent receiver points by distance between them [64 m]. In differential ground motion [Fig. 4b], the vertically propagating body waves and their multiples have been more or less eliminated and only spatial derivative of horizontally travelling seismic phases are present. It means these seismic phases are horizontally travelling surface waves. The generation of surface waves near basin-edge has become very clear in the differential ground motion. Analysis of figure 4 along with very large coherence among the recording stations shows that basin-edge has caused generation of surface waves.

The incident P- and SV-waves have caused generation of Rayleigh waves and incident SH-wave has caused generation of Love wave. Rayleigh waves are recorded in the radial and vertical components and Love waves in the transverse component.

It was also inferred that basin-edge causes significant differential ground motion in addition to the amplification and prolongation of signal. The amplitudes of Rayleigh waves are more than those of causing incident SV-waves in the vertical component. The peak amplitude of surface waves near the edge is varying in a complicated manner due to constructive and destructive interference.

To further verify generation and propagation pattern of surface waves, snapshots of ground displacement at different times were also computed on the ground surface in a rectangular region [2.72 km x 0.8 km] extending from receiver R1 in north-south direction. Figure 5 shows the snapshots of radial, transverse and vertical components of ground displacement at different times. Snapshots at times 2.0 s and 4.0 s depict only P-wave and S-wave and scattered waves near the edge, respectively. The propagation of surface waves in the upper part of the model is observed in next three snapshots taken at 6.0 s, 8.0 s and 10.0 s. Snapshot at time 6.0 s shows only one wavelet of surface waves.

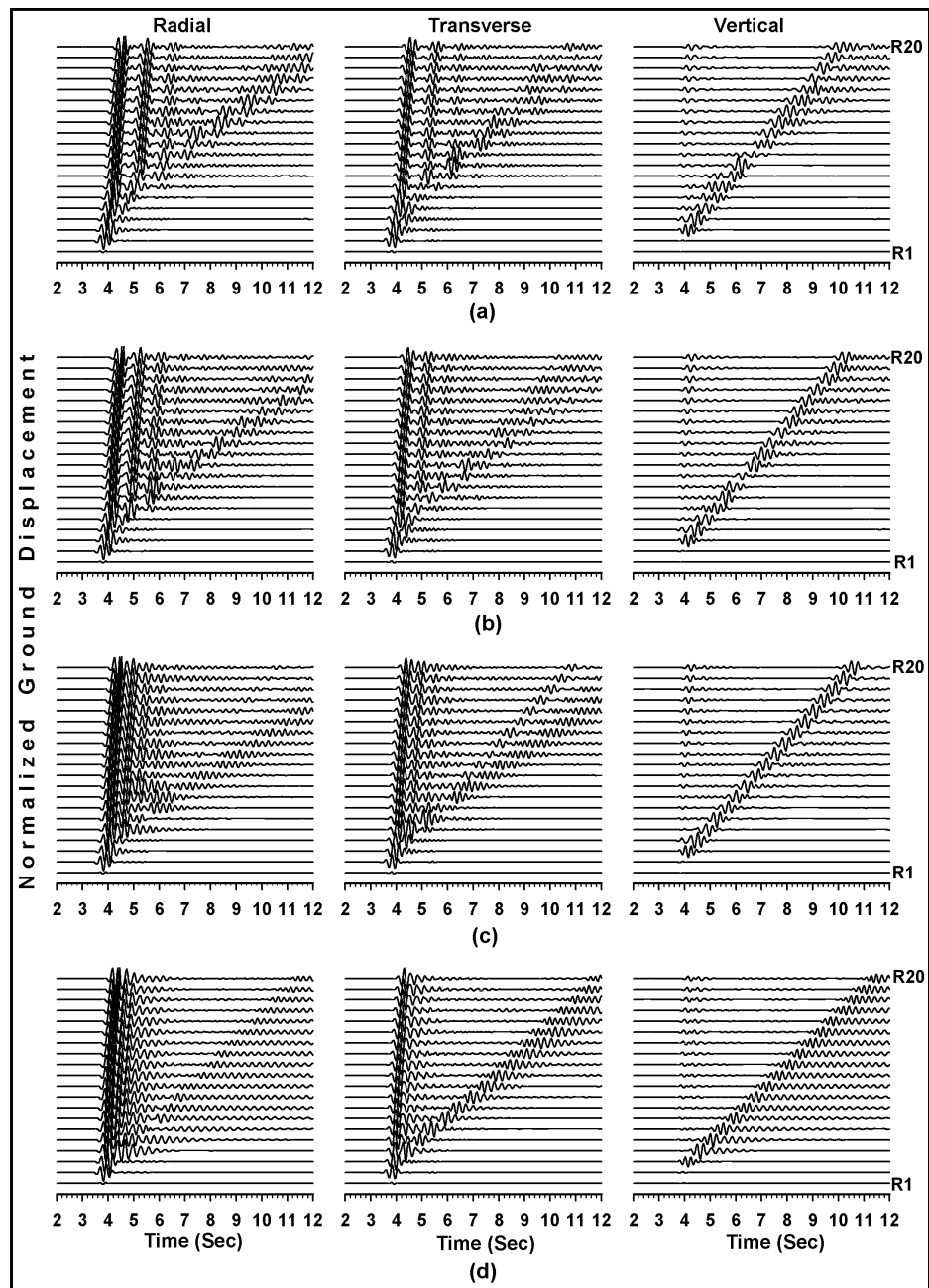


Fig. 6 Radial, transverse and vertical components of responses of the basin-edge model (edge-slope 15°) for different soil thickness using source SL1, (a). 224.0 m, (b). 176.0 m, (c). 128.0 m and (d). 80.0 m.

Slower velocity of Rayleigh waves as compared with Love wave can be inferred on the basis of position of surface waves in snapshots at a particular time. Snapshots at time 8.0 s and 10.0 s clearly indicate two wavelets of both the Rayleigh and Love waves, moving with different velocity. Fast moving Rayleigh wave is more vertically polarised as compared to the slow moving Rayleigh wave. Analysis of figures 4 & 5 and very large coherence among the recording stations reveals that basin-edge has caused strong generation of surface waves.

Effects of soil thickness

Seismic responses of basin-edge model were computed for different soil thickness with edge slope as 15° and source at SL1 [Table 1]. Soil damping was not considered in these simulations. Figure 6 shows the radial, transverse and vertical components of the ground displacement for different thickness of soil [224m, 176m, 128m and 80m]. Surface waves are caused by incident S-waves in all of the cases of soil thickness. The amplitude of Rayleigh wave in vertical component is found to be even more than the causing SV-waves. Figure 6c depicts two modes of both the Rayleigh and Love waves when soil thickness is 128 m, but these modes are not clear in figure 6a and 6b due to presence of longer chain of the body wave multiples. It seems that only fundamental mode has prominently generated when soil thickness was only 80m [Fig. 6d].

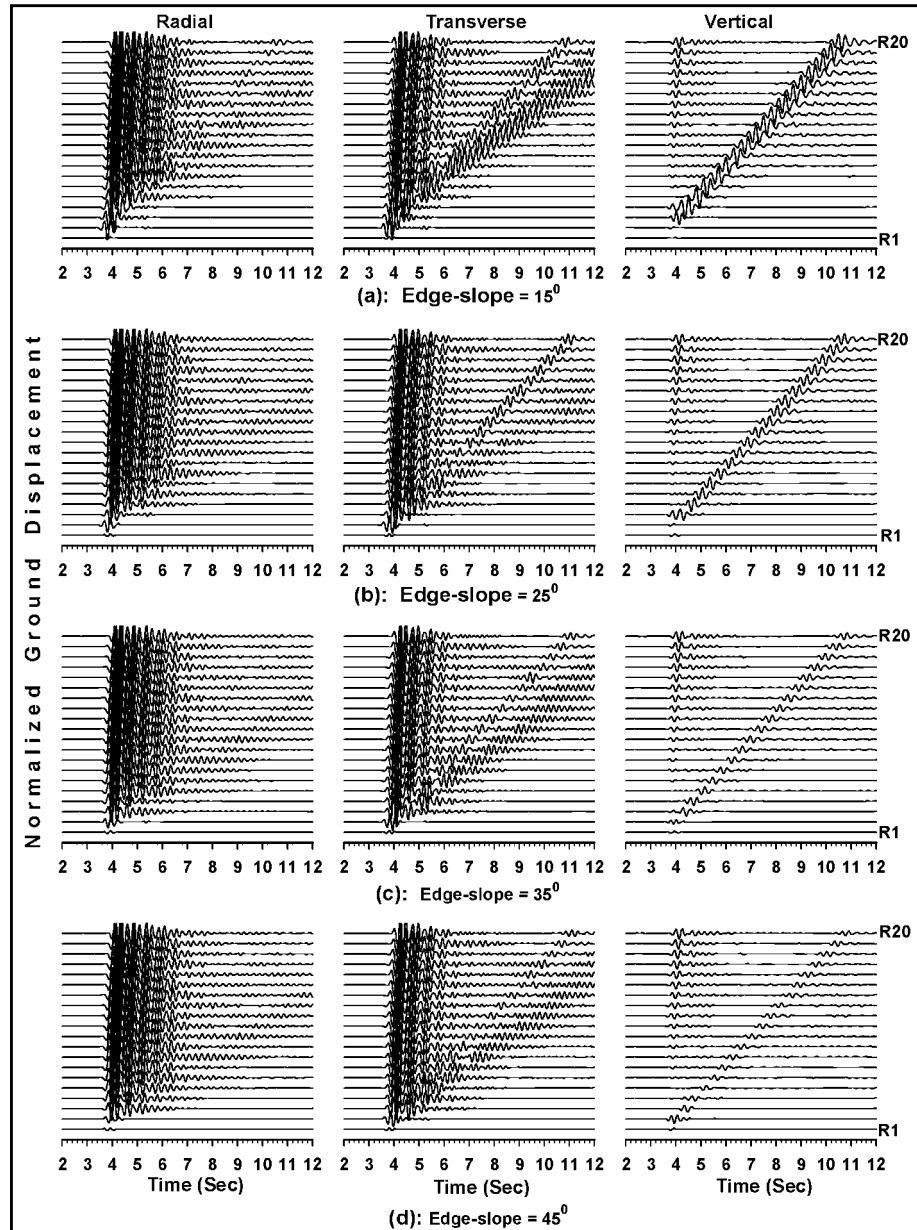


Fig. 7 Radial, transverse and vertical components of responses of the basin-edge model (soil thickness=128 m) for different edge-slope, using source SL2.

Effects of edge-slope

The radial, transverse and vertical components of responses of basin-edge model with soil thickness 128.0 m for different edge-slopes [15° , 25° , 35° and 45°] are shown in figure 7.

This figure reveals decrease of amplitude of surface waves with edge-slope. Spectral amplitudes of surface waves were computed at receiver point R17 for different edge slopes. Figure 8 shows spectral amplitude of Love waves and Rayleigh wave in the transverse component and vertical component, respectively. This figure clearly indicates the decrease of spectral amplitude with edge slope in the vertical component. The spectra of Love wave indicates two bands of frequency, and in both the bands spectral amplitude is more or less decreasing with increase of edge-slope. It also appears that with increase of edge slope the frequency bands are shifting towards higher frequency.

Effects of angle of incidence

To study the effects of angle of incidence on the characteristics of generated surface waves, seismic responses of basin-edge model was simulated using different source locations [Fig. 9]. The source locations, angle of incidence and directions is given in table 1. It is very difficult to compare the characteristics of these surface waves due to variation in amplitude of incoming wave caused by the radiation pattern, even hypo-central distance was kept constant. The moment released per unit volume was same in all the four cases of angle of incidence. Although, surface waves were generated by incident S-waves for all the cases of angle of incidence, but their amplitudes are different, very much dependent on the radiation pattern. Rayleigh waves were also caused by P-waves in figures 9c and 9d, at larger angle of incidence. This may be due to larger amplitude of incident P-waves.

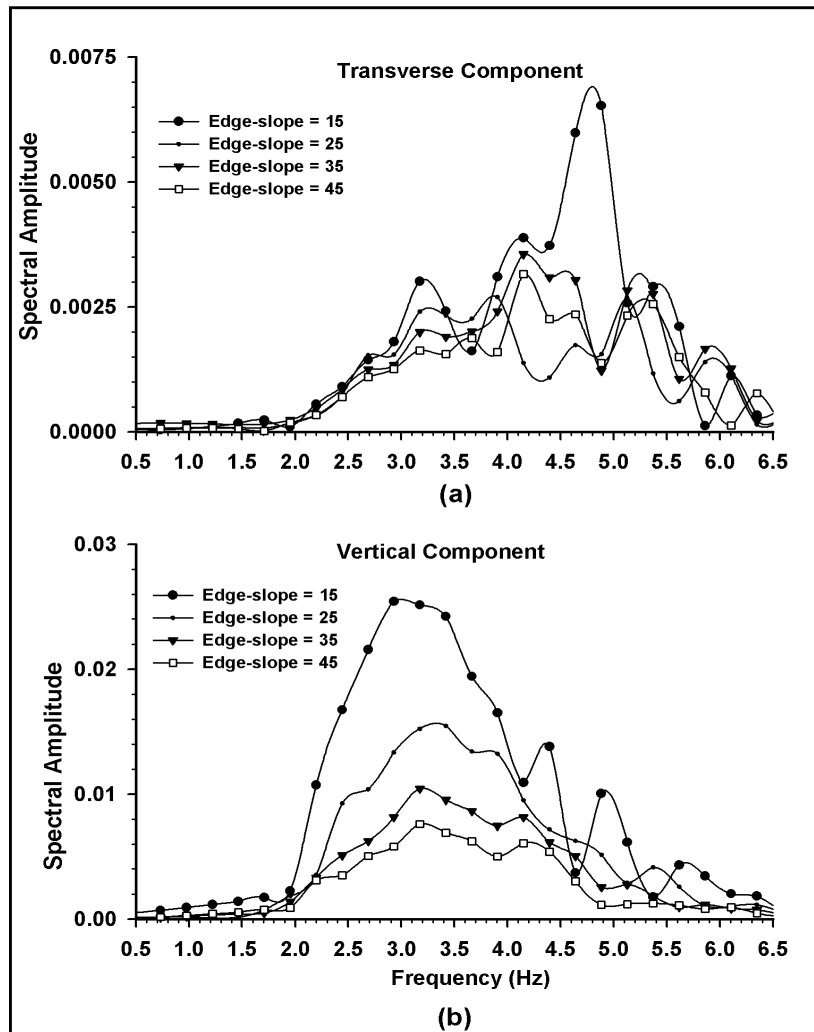


Fig. 8 Spectra of transverse and vertical components of ground displacement corresponding to surface waves recorded on R17 receiver.

DISCUSSION AND CONCLUSIONS

An algorithm developed by Narayan [14] with variable grid size was used in the simulations to study the effects of basin-edge geometry and angle of incidence on the characteristics of generated surface waves.

Large coherence among the recording stations, snapshots, estimated group velocity of the later arrivals and the analysis of differential ground motion revealed that these later arrivals are surface waves who have generated near the basin-edge. The spectral analysis of ground motion corresponding to surface waves revealed generation of high frequency surface wave, near the basin-edge. In addition to the amplification and prolongation of the signal, significant differential ground motion was also obtained. The large ground displacement near the edge in some simulations may be caused by the constructive interference of surface/diffracted waves with the direct waves and their multiples [Kawase [9] and Pitarka [10]].

Higher modes of surface waves were obtained in the case of thicker soil layer. It was inferred that surface wave amplitude decreases with edge slope on the basis of responses of basin-edge models with different edge-slope and spectral analysis. Simulated results for different angle of incidence revealed surface wave generation near the basin-edge in all the cases. Further, it was inferred that the characteristics of these surface waves very much depend on the radiation pattern and to some extent on the angle of incidence. The findings of this paper reveal that basin-edge effects deserve a particular attention for earthquake resistant design and seismic micro-zonation.

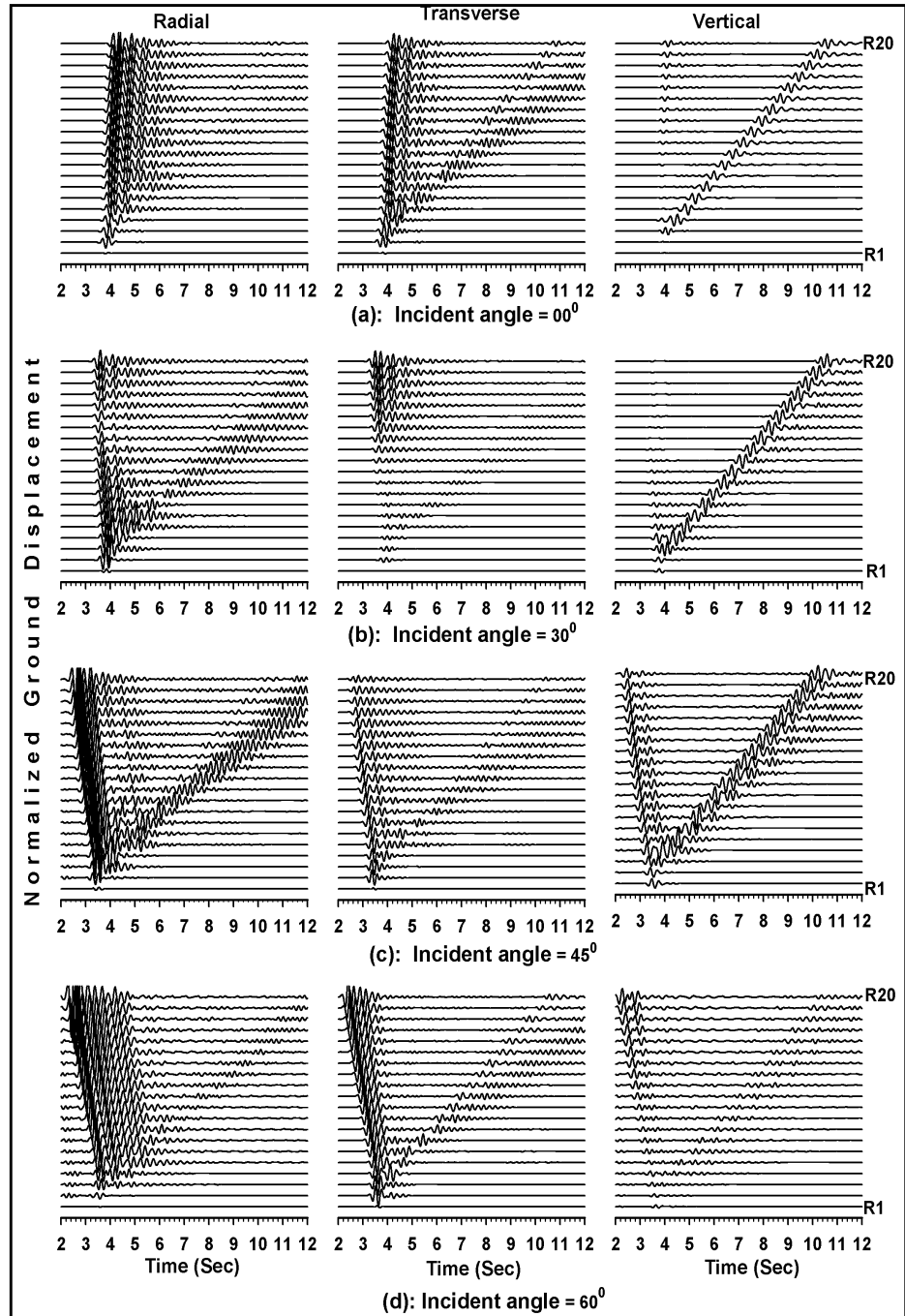


Fig. 9 Radial, transverse and vertical components of responses of the basin-edge model (soil thickness 128 m and slope 15°), using different source locations.

ACKNOWLEDGMENT

Financial assistance by Department of Science and Technology [DST] New Delhi is gratefully acknowledged.

REFERENCES

1. Bard, P.Y., Bouchon, M. "The seismic response of sediment filled valleys, Part 1. The case of incident SH-waves". *Bull. Seism. Soc. Am.*, 1980, 70: 1263-86.
2. Bard, P.Y., Bouchon, M. "The seismic response of sediment filled valleys, Part 2. The case of incident P and SV-waves". *Bull. Seism. Soc. Am.*, 1980, 70: 1921-41.
3. Bard, P.Y., Bouchon, M. "The two-dimensional resonance of sediment filled valleys". *Bull. Seism. Soc. Am.*, 1985, 75: 519-541.
4. Bard, P.Y., Gariel, J.C. "The seismic response of two-dimensional sedimentary deposits with large vertical velocity gradients". *Bull. Seism. Soc. Am.*, 1986, 76: 343-366.
5. Moczo, P., Bard, P.Y. "Wave diffraction, amplification and differential motion near strong lateral discontinuities". *Bull. Seism. Soc. Am.*, 1993, 83: 85-106.
6. Horike, M. "Analysis and simulation of seismic ground motions observed by an array in a sedimentary basin". *J. Phys. Earth*, 1988, 36: 135-154.
7. Kinoshita, S., Fujiwara, H., Mikoshiha, T., Hoshino, T. "Secondary Love waves observed by a strong motion array in the Tokyo lowland". *Japan. J. Phys. Earth*, 1992, 40: 99-116.
8. Hatayama, K., Matsunami, K., Iwata, T., Irikura, K. "Basin-induced Love waves in the eastern part of the Osaka basin". *J. Phys. Earth*, 1995, 43: 131-155.
9. Kawase, H. "The cause of damage belt in Kobe: "The basin-edge effect", constructive interference of the direct S-waves with the basin induced diffracted/Rayleigh waves". *Seism. Res. Lett.*, 1996, 67: 25-34.
10. Pitarka, A., Irikura, K., Iwata, T., Sekiguchi, H. "Three dimensional simulation of the near fault ground motion for 1995, Hyogo-ken Nanbu [Kobe], Japan earthquake". *Bull. Seism. Soc. Am.*, 1998, 88: 428-440.
11. Narayan, J.P. "Study of basin-edge effects on the ground motion characteristics using 2.5d modelling". *Pure Appl. Geophys.*, 2004 [in press].
12. Miyatake, T. "Numerical simulation of earthquake source processes by a three dimensional crack model, Part 1. Rupture process". *J. Phys. Earth*, 1980, 28: 565-598.
13. Pitarka, A. "3D elastic finite difference modelling of seismic motion using staggered grids with nonuniform spacing". *Bull. Seism. Soc. Am.*, 1999, 89: 54-68.
14. Narayan, J.P. "Site-specific ground motion prediction using 3-D modelling". *ISER Jr. of Earthquake Technology*, 2001, 38: 17-29.
15. Narayan, J.P. "Site-specific strong ground motion prediction using 2.5-D modelling". *Geophys. J. Int.*, 2001, 146: 269-281.
16. Graves, R.W. "Simulating seismic wave propagation in 3D elastic media using staggered grid finite difference". *Bull. Seism. Soc. Am.*, 1996, 86: 1091-1106.
17. Israeli, M., Orszag, S.A. "Approximation of radiation boundary conditions". *J. Comp. Phys.*, 1981, 41: 115-135.
18. Luo, Y., Schuster, G. "Parsimonious staggered grid finite differencing of the wave equation". *Geophys. Res. Lett.*, 1990, 17: 155-158.
19. Ohminato, T., Chouet, B. A. "A free surface boundary condition for including 3D topography in the finite difference method". *Bull. Seism. Soc. Am.*, 1997, 87: 494-515.